Chinese Chemical Letters 33 (2022) 890–892

Contents lists available at ScienceDirect

Chinese Chemical Letters

journal homepage: www.elsevier.com/locate/cclet

CoFe-LDH nanowire arrays on graphite felt: A high-performance oxygen evolution electrocatalyst in alkaline media

Biao Deng[a], Jie Liang[b], Luchao Yue[b], Tingshuai Li[b], Qian Liu[c], Yang Liu[d], Shuyan Gao[d], Abdulmohsen Ali Alshehri[e], Khalid Ahmed Alzahrani[e], Yonglan Luo[a,*], Xuping Sun[b,*]

[a] *Chemical Synthesis and Pollution Control Key Laboratory of Sichuan Province, School of Chemistry and Chemical Engineering, China West Normal University, Nanchong 637002, China*
[b] *Institute of Fundamental and Frontier Sciences, University of Electronic Science and Technology of China, Chengdu 610054, China*
[c] *Institute for Advanced Study, Chengdu University, Chengdu 610106, China*
[d] *School of Materials Science and Engineering, Henan Normal University, Xinxiang 453007, China*
[e] *Chemistry Department, Faculty of Science, King Abdulaziz University, P.O. Box 80203, Jeddah 21589, Saudi Arabia*

ARTICLE INFO

Article history:
Received 27 August 2021
Revised 18 September 2021
Accepted 2 October 2021
Available online 7 October 2021

Keywords:
LDH
Graphite felt
Electrocatalyst
Oxygen evolution
Alkaline media

ABSTRACT

Developing non-noble-metal oxygen evolution reaction (OER) electrocatalysts with high performance is critical to electrocatalytic water splitting. In this work, we fabricated CoFe-layered double hydroxide (LDH) nanowire arrays on graphite felt (CoFe-LDH/GF) *via* a hydrothermal method. The CoFe-LDH/GF, as a robust integrated 3D OER anode, exhibits excellent catalytic activity with the need of low overpotential of 252 and 285 mV to drive current densities of 10 and 100 mA/cm^2 in 1.0 mol/L KOH, respectively. In addition, it also maintains electrochemical durability for at least 24 h. This work would open up avenues for the development of GF like attractive catalyst supports for oxygen evolution applications.

Increasing the use of renewable energy and eliminating the consequences of fossil fuels as much as possible are critical issues that scientists urgently need to solve in the future [1,2]. Hydrogen is a promising alternative with the advantages of high energy density and carbon-zero emissions. Water electrolysis provides a facile pathway to produce high-purity hydrogen [3–6]. Unfortunately, the sluggish kinetics of oxygen evolution reaction (OER) is the key limitation for water splitting, which imminently requires efficient water oxidation catalysts (WOCs) to increase the kinetics and obtain high current densities at minimal overpotentials [7–11]. Currently, noble metal oxides catalysts (RuO_2 and IrO_2) demonstrate excellent OER electrocatalytic performance, but scarcity and costliness severely limit their widespread applications [10]. Therefore, the development of highly efficient WOCs made of earth-abundant elements is extremely urgent.

Layered double hydroxide (LDH) has been widely studied as catalysts due to the tunability of microstructure and phase composition [12–18]. Among them, CoFe-LDH as a promising OER electrocatalyst has received extensive attention [19–22]. However, the low electrical conductivity is not favorable for enhanced electrochemical properties for water oxidation catalysis [23,24]. Growing LDH on a conductive substrate is an effective method to solve this problem. Graphite felt (GF) exhibits electrical conductivity (370.37 S/m) close to metal, high volumetric porosity ($\varepsilon < 0.98$), great mechanical integrity and reasonable cost [25–28]. Therefore, GF shows great potential to develop into a frame for self-supporting electrocatalysts. Up to now, there are few pieces of research in this area.

Herein, we report the *in-situ* growth of CoFe-LDH nanowire arrays on GF (CoFe-LDH/GF) through a hydrothermal method. The CoFe-LDH/GF shows excellent OER activity and needs overpotentials (η) of 252 and 285 mV for 10 and 100 mA/cm^2 in 1.0 mol/L KOH, respectively. Moreover, it also maintains electrochemical durability no less than 24 h. The detailed materials preparation is available in Supporting information.

The powder X-ray diffraction (XRD) pattern of CoFe-LDH scraped from GF is shown in Fig. 1a. The diffraction peaks at 11.7°, 23.4°, 34.1°, 36.6°, 38.7°, 43.3°, 46.2°, 59.1° and 60.5° can be assigned to (003), (006), (012), (104), (015), (107), (018), (110) and (113) planes of CoFe-LDH phase (JCPDS No. 50–0235), respectively [29,30]. Fig. S1 (Supporting information) shows the scanning electron microscopy (SEM) images for GF. As shown in Figs. 1b and c, the GF is densely covered by CoFe-LDH nanowire arrays after the hydrothermal treatment. The transmission electron micro-

* Corresponding authors.
E-mail addresses: luoylcwnu@hotmail.com (Y. Luo), xpsun@uestc.edu.cn (X. Sun).

https://doi.org/10.1016/j.cclet.2021.10.002
1001-8417/

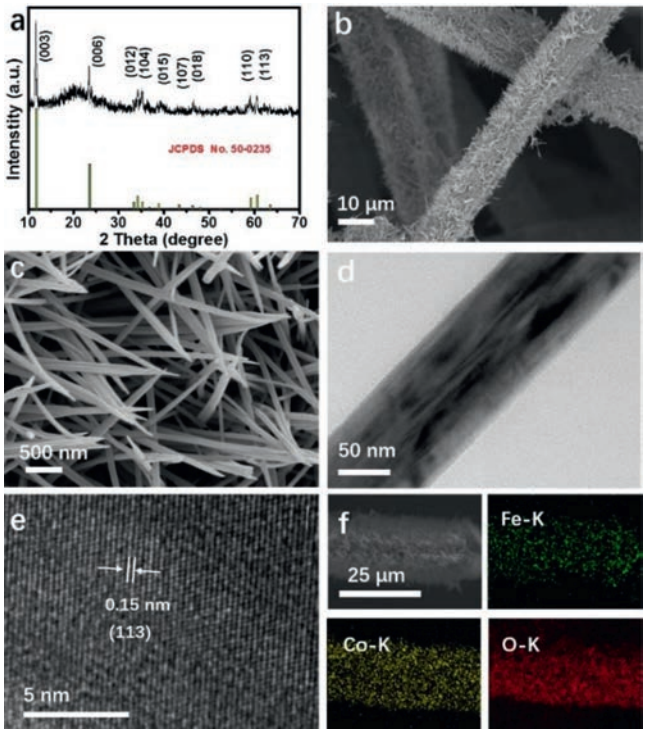

Fig. 1. (a) XRD pattern of CoFe-LDH. (b) Low- and (c) high-magnification SEM images of CoFe-LDH/GF. (d) TEM- and (e) HRTEM images of CoFe-LDH nanowire. (f) SEM and corresponding EDX elemental mapping images of Fe, Co and O for CoFe-LDH/GF.

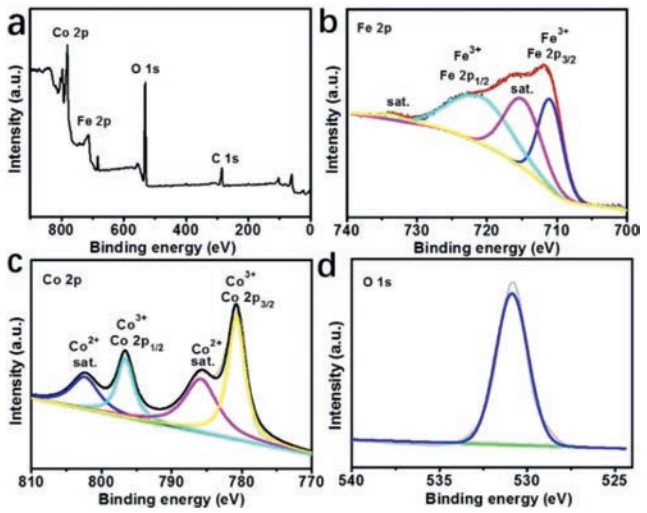

Fig. 2. (a) XPS survey spectrum for CoFe-LDH/GF. XPS spectrum in (b) Fe 2p, (c) Co 2p, and (d) O 1s regions.

scope (TEM) image (Fig. 1d) also strongly supports the formation of nanowire. The high-resolution TEM (HRTEM) image taken from one-single nanowire reveals a lattice spacing value of 0.15 nm, belonging to the (113) plane of CoFe-LDH (Fig. 1e). In addition, the SEM and corresponding energy-dispersive X-ray (EDX) mapping images (Fig. 1f) further demonstrate the uniform distribution of the Fe, Co, and O elements.

X-ray photoelectron spectroscopy (XPS) spectrum of CoFe-LDH/GF indicates typical signals of Fe 2p, Co 2p, O 1s and C 1s (Fig. 2a). In terms of Fe 2p XPS spectrum (Fig. 2b), the two binding energies (BEs) at 724.3 and 710.5 eV are assigned to Fe $2p_{3/2}$ and Fe $2p_{1/2}$ of Fe^{3+}, respectively, along with two satellite peaks

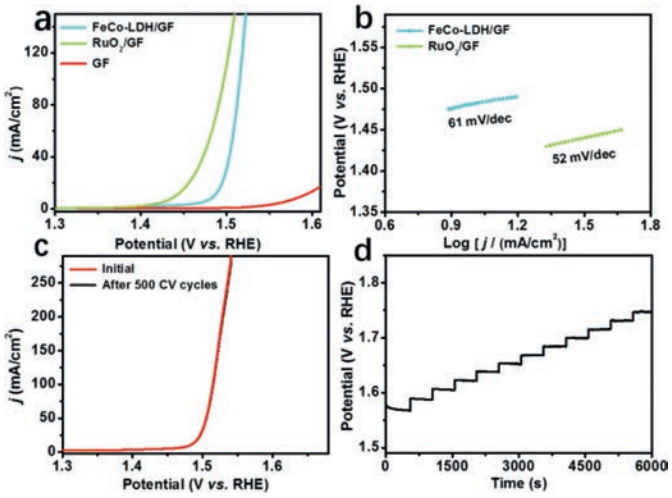

Fig. 3. (a) Polarization curves of CoFe-LDH/GF, RuO_2/GF and GF with a scan rate of 2 mV/s. (b) The corresponding Tafel plots of CoFe-LDH/GF, RuO_2/GF. (c) Polarization curves of CoFe-LDH/GF before and after 500 CV scans. (d) Multi-current process of CoFe-LDH/GF with the current density begins at 40 and ceased at 260 mA/cm^2 with an increment of 20 mA/cm^2 per 500 s.

(716.2 and 733.8 eV) [31,32]. The peak-fitting analysis of Co 2p spectrum (Fig. 2c) displays that there are two BEs of 780.7 and 796.6 eV for Co $2p_{3/2}$ and Co $2p_{1/2}$ of Co^{3+}, respectively. And there are two satellite frequency bands at 786.0 and 801.9 eV in the Co 2p region, implying the existence of a high-spin Co^{2+} state [33]. In the O 1s region (Fig. 2d), the BE of 530.6 eV corresponds to the hydroxyl groups [31].

The electrocatalytic OER activity of CoFe-LDH/GF (loading: 6.5 mg/cm^2) was examined by using a three-electrode configuration in 1.0 mol/L KOH. Meanwhile, bare GF and RuO_2 loaded GF (RuO_2/GF) were also tested for comparison. In addition, all data were *iR*-corrected (except for chronoamperometric tests) to reduce the influence of Ohmic resistance and the applied potentials were converted to the reversible hydrogen electrode (RHE) [34].

Fig. 3a presents the polarization curves of CoFe-LDH/GF, RuO_2/GF and GF. As observed, bare GF has poor OER activity and RuO_2/GF is excellent in OER activity (η = 211 mV at 10 mA/cm^2 and η = 267 mV at 100 mA/cm^2). CoFe-LDH/GF is also highly active for the OER (η = 252 mV at 10 mA/cm^2 and η = 285 mV at 100 mA/cm^2). As shown in Figs. S2a and b (Supporting information), it also shows excellent electrochemical performance in 0.1 mol/L (η = 283 mV at 10 mA/cm^2 and η = 345 mV at 100 mA/cm^2) and 30 wt% KOH (η = 231 mV at 10 mA/cm^2 and η = 257 mV at 100 mA/cm^2). Our CoFe-LDH/GF compares favorably to the behaviors of most reported non-noble-metal OER catalysts in alkaline aqueous media, as listed in Table S1 (Supporting information). The reaction kinetic rate is evaluated by Tafel slope (Fig. 3b). The Tafel slope of CoFe-LDH/GF (61 mV/dec) is close to RuO_2/GF (52 mV/dec), suggesting CoFe-LDH/GF also has fast OER kinetics. Moreover, stability is an important criterion for evaluating electrocatalyst performance. The polarization curve after 500 cyclic voltammetric (CV) scans is almost the same as the initial one, meaning CoFe-LDH/GF possesses high stability (Fig. 3c). Fig. 3d displays the multi-step chronopotentiometric curve of CoFe-LDH/GF with the applied current density gradually increased from 40 mA/cm^2 to 260 mA/cm^2. Under the starting current density, the corresponding potential immediately stabilized at 1.57 V and maintains unchanged for the remaining 500 s. The same results are also observed in other current densities, reflecting superior mass transportation properties, high mechanical robustness, and outstanding electrical conductivity of the CoFe-LDH/GF electrode [35]. The time

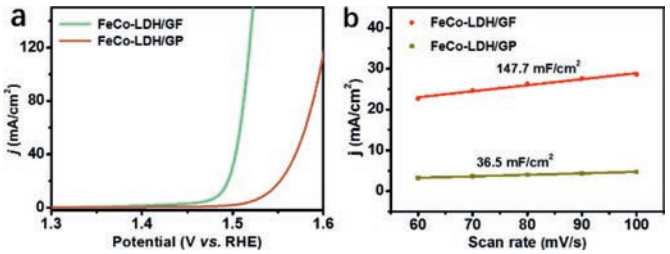

Fig. 4. (a) Polarization curves of CoFe-LDH/GF and CoFe-LDH/GP with a scan rate of 2 mV/s. (b) Double-layer capacitances of CoFe-LDH/GF and CoFe-LDH/GP.

current density curve demonstrates that the CoFe-LDH/GF stably runs over 24 h at a current density of 30 mA/cm^2 (Fig. S3 in Supporting information). CoFe-LDH/GF still maintains its nanowire array morphology (Fig. S4 in Supporting information) after such a prolonged test. Moreover, there is almost no change in the XRD pattern of post-electrolysis CoFe-LDH (Fig. S5 in Supporting information), evidencing the high robustness against OER electrolysis. We further determined the initial pH values and after the durability test (Fig. S6 in Supporting information), pH values remain almost unchanged.

To deeply understand the superiority of the GF, we fabricated CoFe-LDH nanowire arrays on a two-dimensional graphite paper (CoFe-LDH/GP loading: 5.2 mg/cm^2, Fig. S7 in Supporting information) and tested its OER performance. As shown in Fig. 4a, CoFe-LDH/GP demands larger overpotentials to drive the same current densities (η = 307 mV at 10 mA/cm^2 and η = 365 mV at 100 mA/cm^2). As shown in Fig. S8 (Supporting information), the Tafel slope of CoFe-LDH/GP (78 mV/dec) is also higher than that of CoFe-LDH/GF (61 mV/dec), implying the OER kinetics for CoFe-LDH/GP is slower than CoFe-LDH/GF. Notably, compared to CoFe-LDH/GP, CoFe-LDH/GF shows considerably enlarged mass activities (Fig. S9 in Supporting information). The electrochemical active surface area (ECSA) of CoFe-LDH/GF and CoFe-LDH/GP is determined by calculating the double-layer capacitance (C_{dl}). The corresponding cyclic voltammegrams for CoFe-LDH/GF and CoFe-LDH/GP are presented in Fig. S10 (Supporting information). Benefitting from the 3D feature of GF, the C_{dl} value (Fig. 4b) of CoFe-LDH/GF (147.7 mF/cm^2) is about 4 times higher than that of CoFe-LDH/GP (36.5 mF/cm^2), suggesting CoFe-LDH/GF has a larger surface area and thus exposes more active sites for more efficient oxygen evolution electrocatalysis. Electrochemical impedance spectroscopy (EIS) data of CoFe-LDH/GF shows a smaller semicircle radius compared to that of CoFe-LDH/GP (Fig. S11 in Supporting information), suggesting faster electron transfer of CoFe-LDH/GP [36–38].

In conclusion, this study demonstrates the development of CoFe-LDH nanowire arrays on a 3D graphite felt as a catalytic anode for the OER under alkaline conditions. Such CoFe-LDH/GF offers excellent catalytic performance and requires overpotentials of 252 and 285 mV to drive 10 and 100 mA/cm^2, respectively, along with high stability. The whole fabrication process is cost-effective. All these remarkable features, together with the flexible nature of CoFe-LDH/GF, promise its practical use in water-splitting devices.

Declaration of competing interest

We declare that we have no known competing financial interests or personal relationships that could have appeared to influence the work reported in this paper. There is no professional or other personal interest of any nature or kind in any product, service and/or company that could be construed as influencing the position presented in, or the review of, the manuscript entitled.

Acknowledgment

This work was supported by the National Natural Science Foundation of China (No. 22072015).

Supplementary materials

Supplementary material associated with this article can be found, in the online version, at doi:10.1016/j.cclet.2021.10.002.

References

[1] Z. Chen, X. Duan, W. Wei, et al., Nano Res. 13 (2020) 293–314.
[2] L. Jia, B. Liu, Y. Zhao, et al., J. Mater. Sci. 55 (2020) 16197–16210.
[3] X. Li, R. Zhang, Y. Luo, et al., Sustain. Energy Fuels 4 (2020) 3884–3887.
[4] Q. Zhang, Y. Wang, Y. Wang, et al., Chin. Chem. Lett. (2021), doi:10.1016/j.cclet.2021.04.048.
[5] D. Wu, Y. Wei, X. Ren, et al., Adv. Mater. 30 (2018) 1705366.
[6] H. Wang, S. Zhu, J. Deng, et al., Chin. Chem. Lett. 32 (2021) 291–298.
[7] J. Wang, X. Ma, F. Qu, A.M. Asiri, X. Sun, Inorg. Chem. 56 (2017) 1041–1044.
[8] F. Chen, Z. Zhang, W. Liang, et al., Chin. Chem. Lett. (2021), doi:10.1016/j.cclet.2021.08.019.
[9] W. Zhu, R. Zhang, F. Qu, A.M. Asiri, X. Sun, ChemCatChem 9 (2017) 1721–1743.
[10] C. Wang, L. Jin, H. Shang, et al., Chin. Chem. Lett. 32 (2021) 2108–2116.
[11] J. Wang, W. Cui, Q. Liu, et al., Adv. Mater. 28 (2016) 215–230.
[12] C. Ye, L. Zhang, L. Yue, et al., Inorg. Chem. Front. 8 (2021) 3162–3166.
[13] B. Hai, Y. Zou, G. Guo, et al., Chin. Chem. Lett. 28 (2017) 149–152.
[14] P. Ding, C. Meng, J. Liang, Inorg. Chem. 60 (2021) 12703–12708.
[15] M. Wang, Y. Li, J. Ji, et al., Chin. Chem. Lett. 24 (2013) 593–596.
[16] L. Zhang, R. Zhang, R. Ge, et al., Chem. Eur. J. 23 (2017) 11499–11503.
[17] K. Fan, H. Chen, Y. Ji, et al., Nat. Commun. 7 (2016) 11981.
[18] Y. Cao, T. Wang, X. Li, et al., Inorg. Chem. Front. 8 (2021) 3049–3054.
[19] L. Feng, A. Li, Y. Li, et al., ChemPlusChem 82 (2017) 483–488.
[20] P. Ding, F. Luo, P. Wang, et al., J. Mater. Chem. A 8 (2020) 1105–1112.
[21] Y. Liu, Y. Hu, P. Ma, et al., ChemSusChem 12 (2019) 2679–2688.
[22] A. Karmakar, K. Karthick, S. Kumaravel, S.S. Sankar, S. Kundu, Inorg. Chem. 60 (2021) 2023–2036.
[23] Y. Wang, Y. Zhang, Z. Liu, et al., Angew. Chem. Int. Ed. 56 (2017) 5867–5871.
[24] X. Jia, Y. Zhao, G. Chen, et al., Adv. Energy Mater. 6 (2016) 1502585.
[25] L.F. Castaneda, F.C. Walsh, J.L. Nava, C.P.D. Leon, Electrochim. Acta 258 (2017) 1115–1139.
[26] J. Gonzalez-García, P. Bonete, E. Exposito, et al., J. Mater. Chem. 9 (1999) 419–426.
[27] Y. Wang, Y. Liu, K. Wang, et al., Appl. Catal. B: Environ. 165 (2015) 360–368.
[28] S. Zhong, C. Padeste, M. Kazacos, M. Skyllas-Kazacos, J. Power Sources 45 (1993) 29–41.
[29] S.J. Kim, Y. Lee, D.K. Lee, J.W. Lee, J.K. Kang, J. Mater. Chem. A 2 (2014) 4136–4139.
[30] C. Gong, F. Chen, Q. Yang, et al., Chem. Eng. J. 321 (2017) 222–232.
[31] Y. Zhang, M. Yang, X. Jiang, W. Lu, Y. Xing, J. Alloy. Compd. 818 (2020) 153345.
[32] L. Zhong, J. Hu, H. Liang, et al., Adv. Mater. 18 (2006) 2426–2431.
[33] R. Ma, J. Liang, K. Takada, T. Sasaki, J. Am. Chem. Soc. 133 (2011) 613–620.
[34] X. Ji, L. Cui, D. Liu, et al., Chem. Commun. 53 (2017) 3070–3073.
[35] X. Ren, W. Wang, R. Ge, et al., Chem. Commun. 53 (2017) 9000–9003.
[36] S. Chen, F. Bi, K. Xiang, et al., ACS Sustain. Chem. Eng. 7 (2019) 15278–15288.
[37] S. Chen, Y. Yan, P. Hao, et al., ACS Appl. Mater. Interfaces 12 (2020) 12686–12695.
[38] S. Chen, C. Lv, L. Liu, et al., J. Energy Chem. 59 (2021) 212–219.